

A strange metal in a bosonic system

Chao Yang^{1#}, Haiwen Liu^{2#}, Yi Liu³, Jiandong Wang¹, Sishuang Wang¹, Yang Wang¹, Qianmei He¹, Yue Tang³, Jian Wang^{3,4}, X.C. Xie³, James M. Valles Jr.^{5*}, Jie Xiong^{1*} & Yanrong Li^{1,6}

¹State Key Laboratory of Electronic Thin Films and Integrated Devices, University of Electronic Science and Technology of China, Chengdu 610054, China.

²Center for Advanced Quantum Studies, Department of Physics, Beijing Normal University, Beijing 100875, China.

³International Center for Quantum Materials, School of Physics, Peking University, Beijing 100871, China.

⁴Beijing Academy of Quantum Information Sciences, Beijing 100193, China.

⁵Department of Physics, Brown University, 182 Hope Street, Providence, RI 02912, USA.

⁶Sichuan University, Chengdu 610065, China.

#These authors contributed equally to this work.

*Corresponding author. E-mail: jiexiong@uestc.edu.cn (J.X.); james_valles_jr@brown.edu (J.M.V.J).

Abstract

Fermi liquid theory forms the basis for our understanding of the majority of metals, which is manifested in the description of transport properties that the electrical resistivity goes as temperature squared in the limit of zero temperature. However, the observations of strange metal states in various quantum materials^{1–21}, notably high-temperature superconductors^{1–10}, bring this spectacularly successful theoretical framework into crisis. Distinct from the quadratic temperature dependence of the electron scattering rate ($1/\tau$) for ordinary metals, strange metals exhibit resistivity that scales linearly with temperature, indicating that the independent quasiparticle approximation in existing theoretical treatment is no longer valid. When $1/\tau$ hits its limit, $k_B T/\hbar$ where \hbar is the reduced Planck's constant, T represents absolute temperature and k_B denotes Boltzmann's constant, Planckian dissipation^{3,11,12,22–26} occurs and lends strange metals a surprising link to black holes²⁷, gravity^{28–31}, and quantum information theory²⁴. While this strange metal phenomenology originates from investigations of only electronic phases, the centrality of a scattering rate dependent only on fundamental constants raises the question of whether it is exclusive to fermionic systems. Here, we show the characteristic signature of strange metallicity arising unprecedentedly in a bosonic system. Our nanopatterned $\text{YBa}_2\text{Cu}_3\text{O}_{7-\delta}$ (YBCO) film arrays reveal T -linear resistance as well as B -linear magnetoresistance over an extended temperature and magnetic field range in a quantum critical region in the phase diagram. Strikingly, the low-field magnetoresistance oscillates

with a period dictated by the superconducting flux quantum of $h/2e$ where e is the electron charge and h is the Planck constant, indicating that Cooper pairs instead of single electrons dominate the transport process and the system is bosonic. Moreover, the slope of the T -linear resistance α_{cp} appears bounded by $\alpha_{cp} \approx h/2e^2 \cdot 1/T_c^{\text{onset}}$ where T_c^{onset} is the temperature at which Cooper pairs form, intimating a common scale-invariant transport mechanism corresponding to Planckian dissipation. In contrast to fermionic systems where the temperature and magnetic field dependent scattering rates combine in quadrature¹⁵ of $\hbar/\tau \approx \sqrt{((k_B T)^2 + (\mu_B B)^2)}$, both terms linearly combine in the present bosonic system, i.e. $\hbar/\tau \approx (k_B T + \gamma \mu_B B)$, where γ is a constant. By extending the reach of strange metal phenomenology to a bosonic system, our results suggest that there is a fundamental principle governing their transport which transcends particle statistics.

Introduction

The conventional theory of metallic transport predicts that the electrical resistivity $\rho(T)$ at low temperatures should vary as a function of T^2 due to the dominance of electron–electron scattering. However, this common understanding has encountered formidable conceptual challenges in accounting for some recent discoveries. One emerged soon after the discovery of high-temperature superconductors, in the form of a linear temperature dependence of their normal state resistivity over an exceptionally wide range of temperature. Termed by Anderson as one of the central dogmas for condensed matter physics¹, this unusual resistivity versus temperature structure and other anomalous properties signalled the breakdown of the quasiparticle picture in a region of the cuprate phase diagram now referred to as the strange metal phase^{2–12}. Intriguingly, this phase is not confined to cuprates but is also present in many other strongly correlated electron materials, like heavy fermion metals^{13,14,18–21}, pnictides^{15,17}, twisted bilayer graphene¹⁶, organic superconductors¹⁷ and. Strikingly, near the quantum critical point (QCP), the resistance slope appears to be constrained by an upper bound $\alpha_F \approx h/2e^2 \cdot 1/T_F$ where T_F is the Fermi temperature^{1–15,17,18}. This bound corresponds to a scattering rate $1/\tau = k_B T/\hbar$, the so-called Planckian dissipation limit^{11,12,22–26}, which has been received considerable attention recently due to its implications for black holes, gravity, and quantum computation^{27–31}.

Another challenging discovery is the anomalous metallic state in quasi-2D superconducting materials that

appears over a range of magnetic field or normal state resistance^{32–43}. Characterized by saturated residual resistivity near zero temperature, the anomalous metallicity observed in different systems may provide insights necessary for extending our understanding of metals. The fact that Cooper pairs of electrons instead of single electrons dominate the transport in these different anomalous metals leads us to speculate that strange metals might be not restricted to fermionic systems, either.

Here, in a break with the existing pattern that strange metal states are exclusive to systems of fermions, we show that this unusual metallic behavior emerges in a bosonic host and thus the behavior transcends particle statistics. The observed T -linear resistance in a series of nanopatterned YBCO thin films involves clear bosonic transport as evidenced by the period of oscillations in their magnetoresistance. Near the quantum critical point of their superconductor-anomalous metal transition, the slope of the T -linear resistance α_{cp} of the current YBCO strange metal reaches a maximum $\alpha_{\text{cp}} \approx h/2e^2 \cdot 1/T_c^{\text{onset}}$. This apparent bound resembles the one in fermionic systems $\alpha_{\text{F}} \approx h/2e^2 \cdot 1/T_{\text{F}}$ which corresponds to the Planckian dissipation limit and defines the strange metal in their phase diagram. Moreover, the magnetoresistance is linear in this regime with a slope that appears bounded by $\beta_{\text{cp}} \approx h/2e^2 \cdot 1/B^*$ (B^* is a characteristic magnetic field), intimating that a magnetic field introduces an independent and distinct scattering process that is not apparent in fermionic strange metals. Interestingly, the ratio of the slopes $\alpha_{\text{cp}}/\beta_{\text{cp}}$ appears only determined by fundamental constants $2\mu_B/k_B$, indicating scale-invariant behaviors. Our study represents a game-changing step in broadly advancing the conceptual understanding of the mysterious physics of the strange metals.

Results

T -linear resistance

The present studies were conducted on a series of high- T_c superconducting YBCO films nanopatterned with a triangular array of holes. A series of these films with a range of normal state resistances R_{N} , measured just above the superconducting transition temperature, were produced using reactive ion etching (RIE) technique⁴². Nanoporous masks were placed atop pristine 12-nm-thick films and subjected to different etching doses to yield a triangular array of pores that are 103 nm apart and 70 nm in diameter (Supplementary Fig. 1). Increasing etching dose increased R_{N} by inducing more side wall damage in the pores to make the links between array nodes more resistive.

As shown by the sheet resistance as a function of temperature measurements $R_S(T)$ in Fig. 1a, these arrays undergo a superconductor-anomalous metal-insulator transition with increasing R_N . The transport behavior that we focus on occurs in films near the anomalous metal-insulator phase boundary where R_N is close to R_Q . For R_N less than $\sim 3\text{k}\Omega$, the $R_S(T)$ exhibit relatively sharp transitions to a superconducting state starting at an onset temperature T_c^{onset} , that is close to the pristine film transition temperature. As R_N grows larger than $\sim 3\text{k}\Omega$, the anomalous metal phase for which $R_S(T)$ saturates at low temperatures to a constant value appears⁴² (Supplementary Fig. 2). When R_N approaches $12\text{k}\Omega$, near the anomalous metal-insulator transition point, the $R_S(T)$ develops a nearly linear temperature dependence over an extended range, as shown by five representative samples, f1–f5. Strikingly, in the case of f3 (R_N approaches $12\text{k}\Omega$) the linear temperature dependence extends over a factor for 20 in temperature from 60 K to 3 K with a low-temperature intercept near zero. Above $12\text{k}\Omega$, the linear temperature dependence develops into an insulating dependence (i.e. $dR/dT < 0$) in the low-temperature limit.

Having detected a regime with T -linear resistance, we now turn to investigate its slope. Denoting it as $\alpha_{\text{cp}} = dR_S(T)/dT$, we introduce a normalized form $\eta = (2e^2/h) \cdot \alpha_{\text{cp}} T_c^{\text{onset}}$, inspired by $\eta = 2e^2/h \cdot \alpha_F T_F$ in fermionic systems⁷. The extracted α_{cp} and η values for each sample measured in Fig. 1a are plotted against R_N in Fig. 1b. The slope peaks at a value of $\alpha_{\text{cp}} \approx 157\ \Omega\ \text{K}^{-1}$ and $\alpha = 1.02$ for the film f3 exhibiting the greatest range of T -linear resistance. Over the R_N range bracketing f3, $10\text{k}\Omega$ to $15\text{k}\Omega$, the slope remains within 25% of the maximum value while the lowest temperature behaviors of the $R_S(T)$ evolve from anomalous metal (e.g. f1 and f2) to insulator (e.g. f5).

Bosonic nature

Information about the charge carriers producing the linear resistance comes from the low magnetic field magneto-resistance. Below T_c^{onset} , the magnetoresistances of the nanopatterned thin films (Fig. 1c and Supplementary Fig. 3) oscillate with a constant period of $\mu_0 H_{\text{period}} \approx 0.225\text{T}$, corresponding to one superconducting flux quantum per unit cell of the array with $H_{\text{period}} \approx h/2eS$ and the unit cell area $S \approx 9200\ \text{nm}^2$. These quantum oscillations below T_c^{onset} provide direct evidence that Cooper pairs instead of single electrons dominate the transport process^{42,44}.

B-linear resistance

The T -linear resistance persists in magnetic fields ($B > 1$ T) beyond the magnetoresistance oscillations, as shown in Fig. 2a–c. The magnetoresistance is uniformly positive up to the measurement limit of 9T. Examining the magneto-resistance directly reveals that it is nearly linear over this field scale for a wide range of temperatures (Fig. 2d, e and Supplementary Fig. 4). By contrast, the magneto-resistance for the lower R_N superconducting (SC) sample is non-linear (Fig. 2f). Notably, the linear magneto-resistance curves of samples f1–f5 are approximately parallel for a wide range of temperatures. Their slopes obtained from linear fits, $\beta_{cp} = \frac{dR}{dB}$, as a function of temperature capture this observation (Fig. 2g, h and Supplementary Fig. 5). β_{cp} for film f4, for example, shows a plateau over which it varies by only 12% from 30K to 2K, while its resistance changes by almost a factor of 3 as shown in Fig. 2g. The temperature range for this plateau or broad peak coincides with the temperature range over which the resistance is linearly temperature dependent. Writing the magnetoresistance in a form similar to the temperature dependence $\frac{dR}{dB} = \frac{h}{2e^2} \cdot \frac{1}{B^*}$, we can identify a magnetic field scale B^* for the slope. At the maximum slope, B^* is approximately 60 T.

The linear dependencies of the sheet resistance on T and B indicates that:

$$(R_S(T, B) - R_S(0,0))/T = \alpha_{cp} + \beta_{cp} \cdot \frac{B}{T} \quad (1)$$

over a wide temperature and magnetic field range. Replotting the $R_S(T, B)$ as $(R_S(T, B) - R_S(0,0))/T$ vs. $\frac{B}{T}$ leads to the collapse onto a single curve from 3 K to 30 K as shown for f4 in Fig. 3a. The scaling plot of other samples are shown in Fig. 3b and Supplementary Fig. 6. The ratio of β_{cp} and α_{cp} gives a quantity that is very close to a ratio of fundamental constants $k_B/\gamma\mu_B$, where γ is a dimensionless parameter, and μ_B is Bohr magneton.

Phase diagram

To depict the region over which the scaling appears to hold, we plot $1/R_N \cdot d^2R_S/dT^2$ on a color scale on R_N versus T axes, as shown in Fig. 4a. This region is represented by the wide green region in the central part Fig. 4a, where $1/R_N \cdot d^2R_S/dT^2$ is near zero. It funnels down with decreasing temperature from T_c^{onset}

becoming narrow near the critical sheet resistance $R_{NC} \sim h/2e^2$ separating the insulating and anomalous metal phases at low temperatures. We label this green area as the bosonic strange metal, reminiscent of the strange metal in fermionic systems.

Discussion

The present work uncovers a distinctive bosonic metallic transport behavior that deviates from the previous boson localization paradigm of the superconductor-insulator transition in which metallic behavior appears with a critical resistance R_Q at a critical point of a tuning parameter like magnetic field or normal state resistance. Like the anomalous metal state, this strange metal state exists over a range of tuning parameters with residual resistances far below R_Q . The primary characteristics that distinguish this bosonic transport behavior are 1) a resistance that changes linearly with temperature with a slope that appears bounded by a quantum of resistance and is inversely proportional to an energy scale characterizing the ground state of the charge carriers, 2) a magnetoresistance that changes linearly with magnetic field as implied by the data collapse in Fig. 3, and 3) the appearance of these behaviors in a fan-shaped region that appears to terminate in a quantum critical point in the phase diagram in Fig. 4.

Because these bosonic transport characteristics are similar to the fermionic strange metals¹⁻¹⁹, we discuss them in that context first. In the model based on the Drude approach, the scattering rate is presumed to reach and be bounded by the so-called Planckian dissipation limit, $1/\tau = k_B T/\hbar$. The slope of the sheet resistance, $\alpha = (m^*/ne^2)(k_B/\hbar)$ then only depends on m^*/n where m^* is the effective mass and n is the carrier density. For the fermionic systems, n/m^* is proportional to T_F in a two-dimensional approximation. For Cooper pairs as the carriers, T_c^{onset} , which measures the portion of the Fermi volume that forms pairs serves as the appropriate energy scale. Thus, the linear temperature dependence of the bosonic system is much larger than the fermionic systems by the ratio T_F/T_c^{onset} , in accord with the data (also see Table 1). Turning to the magnetic field dependence, fermionic systems show $\hbar/\tau \approx \sqrt{((k_B T)^2 + (\mu_B B)^2)}$ in some cases¹⁵. This scale free form indicates that the scattering does not depend directly on any intrinsic energy scale characteristic of the systems. The data for the bosonic system here are also consistent with a scale free scattering rate with $\hbar/\tau \approx k_B T + \gamma \mu_B B$ with $\gamma \approx 2$. This form, in contrast to the quadrature form for the fermionic case, implies that there are two independent scattering processes.

Reminiscent of Planckian dissipation $\hbar/\tau_1 \approx k_B T$, it implies a magnetic field damping rate $\hbar/\tau_2 \approx \gamma \mu_B B$, namely, the type-II Planckian dissipation. This conjecture relies on the experimental observation that $\gamma = \frac{k_B T_c^{\text{onset}}}{\mu_B B^*}$, which is remarkably close to the Landau g factor.

Viewing this novel behavior within the context of the natural model for these arrays, the quantum XY model with dissipation provides an explanation for why this novel behavior has not been observed before. The dissipative processes involve the coupling of the bosons to low-lying fermionic excitations of this d-wave system^{42,45}. This dissipative model can exhibit critical behavior⁴⁶ that differs from the non-dissipative models⁴⁷. It has three, rather than two, ground states: an ordered superconducting state, a disordered insulating state and in between a quasi-ordered state that is of interest here^{48,49}. The phase of the order parameter in the less familiar quasi-ordered state is spatially ordered and temporally disordered^{48,49}. Here, we tune the normal resistance R_N to cross the three phases. Estimates of the model parameters based on the geometry of these arrays and a standard form for the Josephson coupling energy between array nodes leads to the identification of the phases at different R_N that is shown in Fig. 4b. The absence of reports of strange metal behavior in prior superconducting array experiments suggests that its emergence here is related to the high- T_c superconducting state. Previous investigations employed primarily s-wave superconductors, which afford fewer of the low energy excitations for the dissipation necessary to enter the critical region described above. Also, their anomalous metal behaviors appear at significantly lower R_N where the BKT transition appears closer to T_c^{onset} ³². While this explanation is appealing, it could be that the higher T_c^{onset} made the linear- T resistance more apparent as it extends over a decade in temperature.

Future measurements of the frequency dependent conductivity show promise for direct insights into the dynamics of this system that could reveal the origins of these linear transport phenomena. A measurement of the Drude width can be particularly interesting as it has been proposed to scale with the entropy in models proposed to apply to matter in many forms including cold atoms, the solid-state materials and quark gluon plasmas. In addition, as dissipation induced decoherence processes are important in quantum computing, our results provide a platform for further study of the dissipative quantum system.

Methods

Sample preparation

The high- T_c $\text{YBa}_2\text{Cu}_3\text{O}_{7-\delta}$ superconducting films were epitaxial grown on (001)-oriented substrates SrTiO_3 in a dc magnetron sputtering system. The films were grown in an argon/oxygen (ratio 2:1) mixture under the working pressure of 30 Pa at $T \approx 700^\circ\text{C}$, with a very low growth rate ($\sim 0.8 \text{ nm min}^{-1}$). Then, an anodic aluminum oxide (AAO) template of 200 nm thick was transferred to YBCO thin film. By reactive ion etching, the AAO pattern of a triangular array of holes with a 70-nm diameter and 103-nm period is duplicated onto the YBCO films. The etching recipe includes 30 sccm CHF_3 , 40 sccm Ar, 20 mTorr (1 Torr ≈ 133 Pa) pressure, 200 W rf power, 1800W inductive coupling plasma (ICP). The YBCO films can be tuned from superconducting state to an insulating state by increasing the etching time from 20s to 160s⁴².

Measurements

The in-plane resistance and magnetoresistance were measured with a standard four-probe in a commercial Physical Property Measurement System (PPMS, Quantum Design) with magnetic fields up to 9 T. The size of YBCO samples for the measurements is typically $1 \text{ cm} \times 1 \text{ cm}$. For the transport measurements, the excitation electrical current as low as possible (5 nA \sim 500 nA) was applied in the ab-plane while the magnetic field was applied along the c-axis. The sweeping rate is typically 0.04 T min^{-1} for measuring the magnetoresistance quantum oscillations.

References

1. Anderson, P. W. *The Theory of Superconductivity in the High- T_c Cuprates* (Princeton University Press, Princeton, 1998).
2. Keimer, B., Kivelson, S. A., Norman, M. R., Uchida, S. & Zaanen, J. From quantum matter to high-temperature superconductivity in copper oxides. *Nature*, **518**, 179–186 (2015).
3. Zaanen, J. Why the temperature is high. *Nature* **430**, 512–513 (2004).
4. Jin, K., Butch, N. P., Kirshenbaum, K., Paglione, J. & Greene, R. L. Link between spin fluctuations and electron pairing in copper oxide superconductors. *Nature* **476**, 73–75 (2011).
5. Greene, R. L. The Strange Metal State of the Electron-Doped Cuprates *Annu. Rev. Condens. Matter Phys.* **11**, 213–229 (2020).
6. Taillefer, L. Scattering and Pairing in Cuprate Superconductors. *Annu. Rev. Condens. Matter Phys.* **1**, 51–70 (2010).
7. Giraldo-Gallo, P. et al. Scale-invariant magnetoresistance in a cuprate superconductor. *Science* **361**, 479–481 (2018).
8. Legros, A. et al. Universal T -linear resistivity and Planckian dissipation in overdoped cuprates. *Nat. Phys.* **15**, 142–147 (2019).
9. Varma, C. M., Littlewood, P. B., Schmitt-Rink, S., Abrahams, E., & Ruckenstein, A. E. Phenomenology of the normal state of Cu-O high-temperature superconductors. *Phys. Rev. Lett.* **63**, 1996–1999 (1989).
10. Varma, C. M. Linear in temperature resistivity and associated mysteries including high temperature superconductivity. *Rev. Mod. Phys.* **92**, 031001 (2020).
11. Hartnoll, S. A. Theory of universal incoherent metallic transport. *Nat. Phys.* **11**, 54–61 (2015).
12. Patel A. A. & Sachdev, S. Theory of a Planckian Metal. *Phys. Rev. Lett.* **123**, 066601 (2019).
13. Tomita, T., Kuga, K., Uwatoko, Y., Coleman, P., & Nakatsuji, S. Strange metal without magnetic criticality.

- Science* **349**, 506–509 (2015).
14. Shen, B. Strange-metal behaviour in a pure ferromagnetic Kondo lattice. *Nature* **579**, 51–55 (2020).
 15. Hayes, I. M. et al. Scaling between magnetic field and temperature in the high-temperature superconductor $\text{BaFe}_2(\text{As}_{1-x}\text{P}_x)_2$. *Nat. Phys.* **12**, 916–919 (2016).
 16. Cao, Y. et al. Strange metal in magic-angle graphene with near Planckian dissipation. *Phys. Rev. Lett.* **124**, 076801 (2020).
 17. Doiron-Leyraud, N. et al. Correlation between linear resistivity and T_c in the Bechgaard salts and the pnictide superconductor $\text{Ba}(\text{Fe}_{1-x}\text{Co}_x)_2\text{As}_2$. *Phys. Rev. B* **80**, 214531 (2009).
 18. Bruin, J. A. N., Sakai, H., Perry, R. S. & Mackenzie, A. P. Similarity of scattering rates in metals showing T -linear resistivity. *Science* **339**, 804–807 (2013).
 19. Custers, J. The break-up of heavy electrons at a quantum critical point. *Nature* **424**, 524–527 (2003).
 20. Gegenwart, P., Si, Q. & Steglich, F. Quantum criticality in heavy-fermion metals. *Nature Physics* **4**, 186–197 (2008).
 21. Prochaska, L. Singular charge fluctuations at a magnetic quantum critical point. *Science* **367**, 285–288 (2020).
 22. Hartnoll, S. A. & Hofman, D. M. Locally critical resistivities from Umklapp scattering. *Phys. Rev. Lett.* **108**, 241601 (2012).
 23. Zaanen, J. Electrons go with the flow in exotic material systems. *Science* **351**, 1026–1027 (2016).
 24. Zaanen, J. Planckian dissipation, minimal viscosity and the transport in cuprate strange metals. *SciPost Phys.* **6**, 061 (2019).
 25. Brown, P. T. et al. Bad metallic transport in a cold atom Fermi-Hubbard system. *Science* **363**, 379–382 (2019).
 26. Cao, C. et al. Universal quantum viscosity in a unitary Fermi gas. *Science* **331**, 58–61 (2010).
 27. Kovtun, P. K., Son, D. T. & Starinets, A. O. Viscosity in strongly interacting quantum field theories from black hole physics. *Phys. Rev. Lett.* **94**, 111601 (2005).
 28. Faulkner, T. et al. Strange Metal Transport Realized by Gauge/Gravity Duality. *Science* **329**, 4013–4047 (2010).
 29. Davison, R. A., Schalm K. & Zaanen, J. Holographic duality and the resistivity of strange metals. *Phys. Rev. B* **89**, 245116 (2014).
 30. Zaanen, J., Liu, Y., Sun, Y. & Schalm, K. *Holographic Duality in Condensed Matter Physics* (Cambridge University Press, Cambridge, 2015).
 31. Hartnoll, S. A., Lucas, A. & Sachdev, S. Holographic quantum matter. Preprint at <https://arxiv.org/abs/1612.07324v1> (2016).
 32. Kapitulnik, A., Kivelson, S. A. & Spivak, B. *Colloquium: Anomalous metals: Failed superconductors*. *Rev. Mod. Phys.* **91**, 011002 (2019).
 33. Doniach, S. & Das, D. The bose metal: a commentary. *Brazilian Journal of Physics* **33**, 740-743 (2003).
 34. Phillips, P. & Dalidovich, D. The elusive Bose metal. *Science* **302**, 243–247 (2003).
 35. Jaeger, H. M., Haviland, D. B., Orr, B. G. & Goldman, A. M. Onset of superconductivity in ultrathin granular metal films. *Phys. Rev. B Condens. Matter* **40**, 182–196 (1989).
 36. Mason, N. & Kapitulnik, A. Dissipation Effects on the Superconductor-Insulator Transition in 2D Superconductors. *Phys. Rev. Lett.* **82**, 5341–5344 (1999).
 37. Garcia-Barriocanal, J. et al. Electronically driven superconductor-insulator transition in electrostatically doped $\text{La}_2\text{CuO}_{4+\delta}$ thin films. *Phys. Rev. B Condens. Matter Mater. Phys.* **87**, 024509 (2013).
 38. Han, Z. et al. Collapse of superconductivity in a hybrid tin–graphene Josephson junction array. *Nat. Phys.*

- 10, 380–386 (2014).
39. Saito, Y., Kasahara, Y., Ye, J., Iwasa, Y. & Nojima, T. Metallic ground state in an ion-gated two-dimensional superconductor. *Science* **350**, 409–413 (2015).
 40. Böttcher, C. G. L. et al. Superconducting, insulating and anomalous metallic regimes in a gated two-dimensional semiconductor–superconductor array. *Nat. Phys.* **14**, 1138–1144 (2018).
 41. Breznay, N. P. & Kapitulnik, A., Particle-hole symmetry reveals failed superconductivity in the metallic phase of two-dimensional superconducting films. *Sci. Adv.* **3**, e1700612 (2017).
 42. Yang, C. et al. Intermediate bosonic metallic state in the superconductor-insulator transition. *Science* **366**, 1505–1509 (2019).
 43. Liu, Y. et al. Type-II Ising superconductivity and anomalous metallic state in macro-size ambient-stable ultrathin crystalline films. *Nano Letters* **20**, 5728–5734 (2020)
 44. Stewart Jr, M. D., Yin, A., Xu, J. M., Valles Jr, J. M. Superconducting pair correlations in an amorphous insulating nanohoneycomb film. *Science* **318**, 1273–1275 (2007).
 45. Eckern, U., Schön, G., & Ambegaokar, V. Quantum dynamics of a superconducting tunnel junction. *Phys. Rev. B* **30**, 6419–6431 (1984).
 46. Chakravarty, S. *Understanding Quantum Phase Transitions* (CRC Press, Florida, 2010).
 47. Fisher, M. P. A., Weichman, P. B., Grinstein, G. & Fisher, D. S. Boson localization and the superfluid-insulator transition. *Phys. Rev. B* **40**, 546–570 (1989).
 48. Vivek Aji & Varma C. M. Theory of the Quantum Critical Fluctuations in Cuprate Superconductors. *Phys. Rev. Lett.* **99**, 067003 (2007).
 49. Zhu, L., Hou, C. & Varma, C. M. Quantum criticality in the two-dimensional dissipative quantum XY model. *Phys. Rev. B* **94**, 235156 (2016).

Acknowledgements

The authors would like to thank C. M. Varma, H. Yao, A. Lucas, and J. M. Kosterlitz for the fruitful discussions. This work was supported by the National Natural Science Foundation of China (grant 51722204, 11888101, 50902017, U20A20244, 12022407, and 11774008), the National Basic Research Program of China (grant 2018YFA0305604, 2017YFA0303300, and 2017YFA0304600), Beijing Natural Science Foundation (Z180010).

Author contributions

J.X. and J.M.V.J. conceived the study and supervised the project together with Y.L. and J.W.. C.Y. and JIAND.W. fabricated the samples. C.Y., Y.LIU., S.W., Y.W., Q.H. and Y.T. performed the experimental measurements. C.Y., H.L., J.M.V.J. and J.X. analyzed the data with the contribution of Y.LIU., J.W. and Y.L.. X.C.X. participated in discussions. C.Y., J.M.V.J., H.L, J.X. and Y.L. wrote the manuscript with comments from J.W..

Competing interests

The authors declare no competing interests.

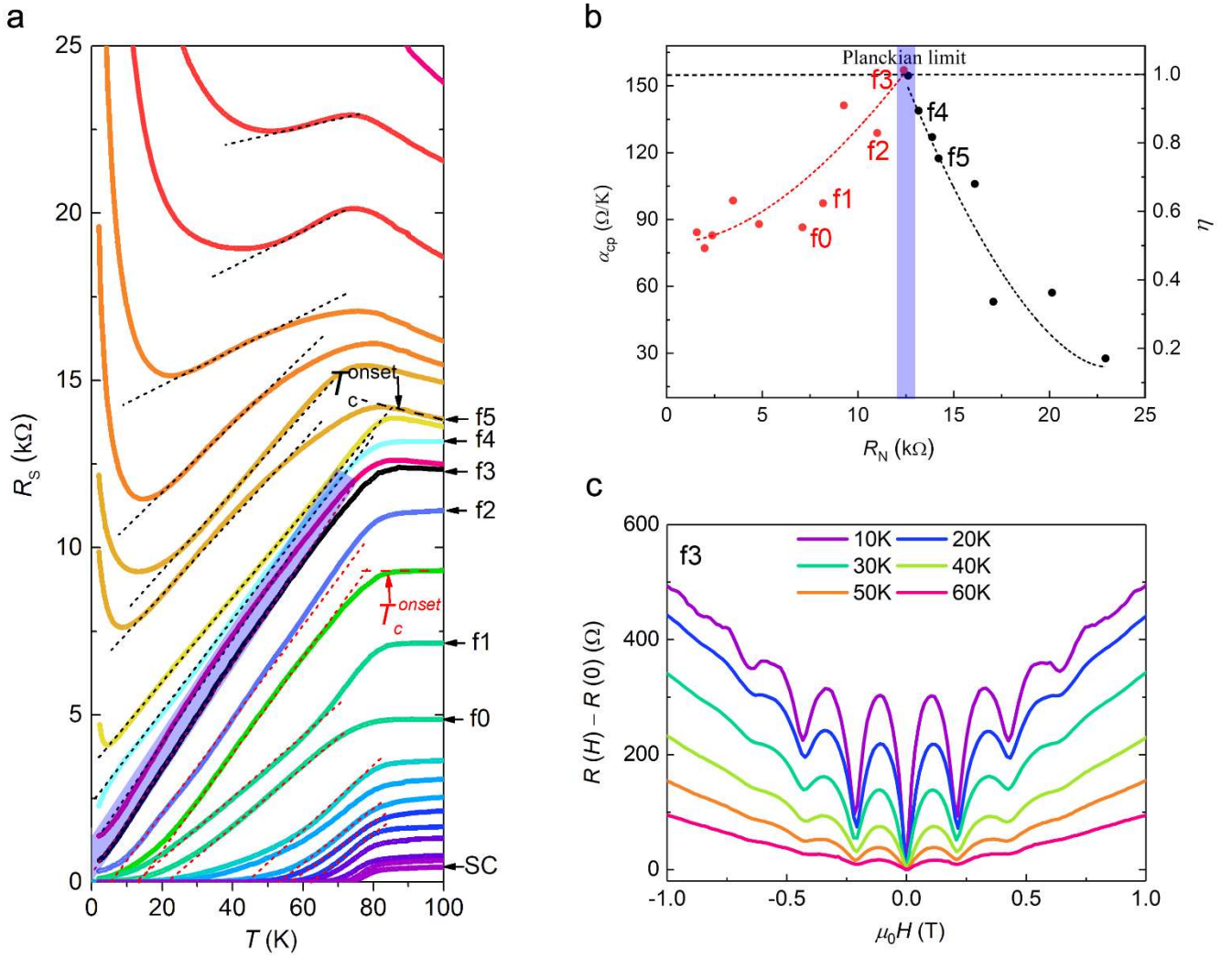


Fig. 1] Linear-in-temperature resistance near a bosonic anomalous metal-insulator transition in nanopatterned YBCO thin films. (a) Sheet resistance as a function of temperature $R_S(T)$ for a series of nanopatterned YBCO films over a range of normal state sheet resistances R_N . The dashed lines are linear fits to the data to determine the slope α_{cp} of the linear portion of the $R_S(T)$ that develops for R_N close to R_Q . Close to the transition point of anomalous metal-insulator transition, the resistance shows linear temperature dependence from around 60 K down to around 3 K. **(b)** Slopes α_{cp} in a) as a function of R_N . The right axis η is the slope normalized by $(2e^2/h) \cdot T_c^{\text{onset}}$, where T_c^{onset} is defined by the construction shown. The maximum observed slope, deemed the Planckian limit, corresponds to $\eta=1$. **(c)** Low field magnetoresistance of film f3 ($R_N \sim h/2e^2$) as a function of temperature. The damped oscillations have a period $\mu_0 H_0 \sim 0.225$ T corresponding to one charge $2e$ flux quantum per unit cell of the array. (other representative films are shown in Supplementary Fig. 3).

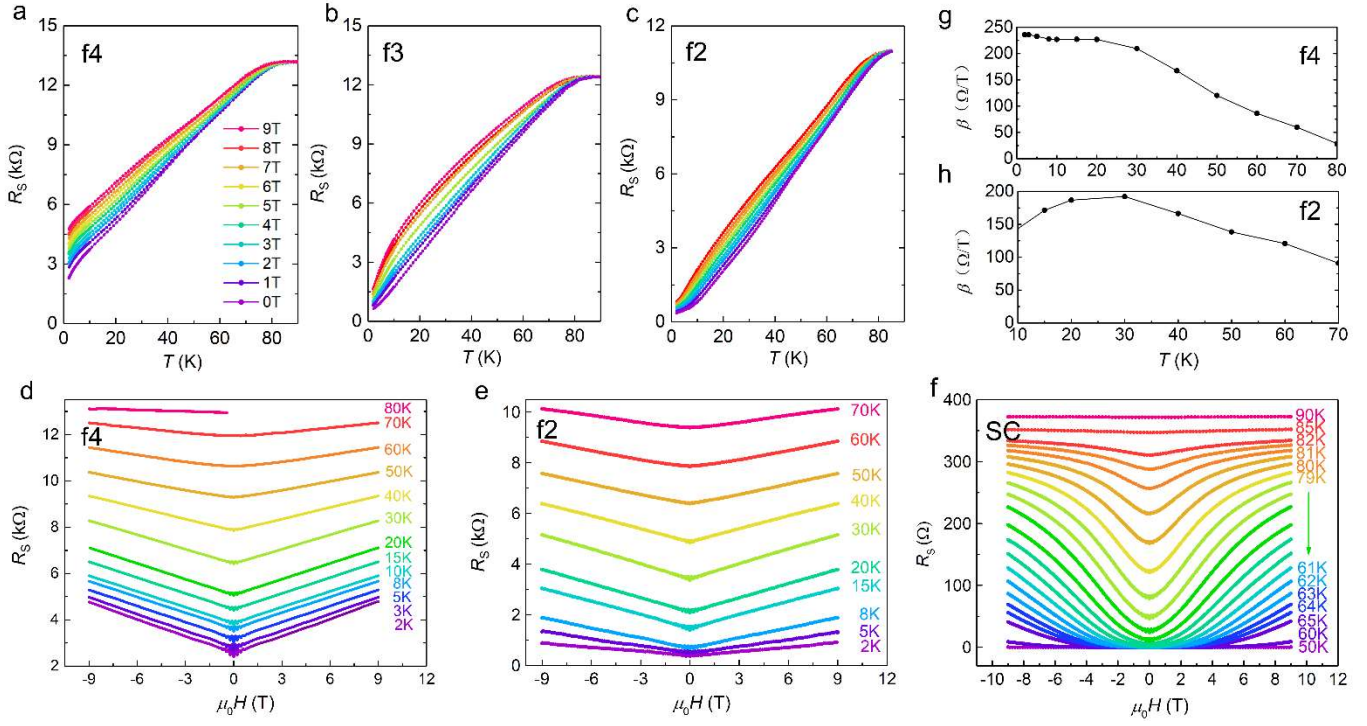


Fig. 2 | T -linear resistance and scale-invariant B -linear resistance in nanopatterned YBCO thin films under perpendicular magnetic field. (a–c) $R_s(T)$ curves for films: f4 (a), f3 (b), f2 (c), under different perpendicular magnetic fields indicated by the legend in (a). (d–f) The magnetoresistance for films: f4 (d), f2 (e), SC (f). The slope of magnetoresistance β of f4 (a) and f2 (d) as a function of temperature.

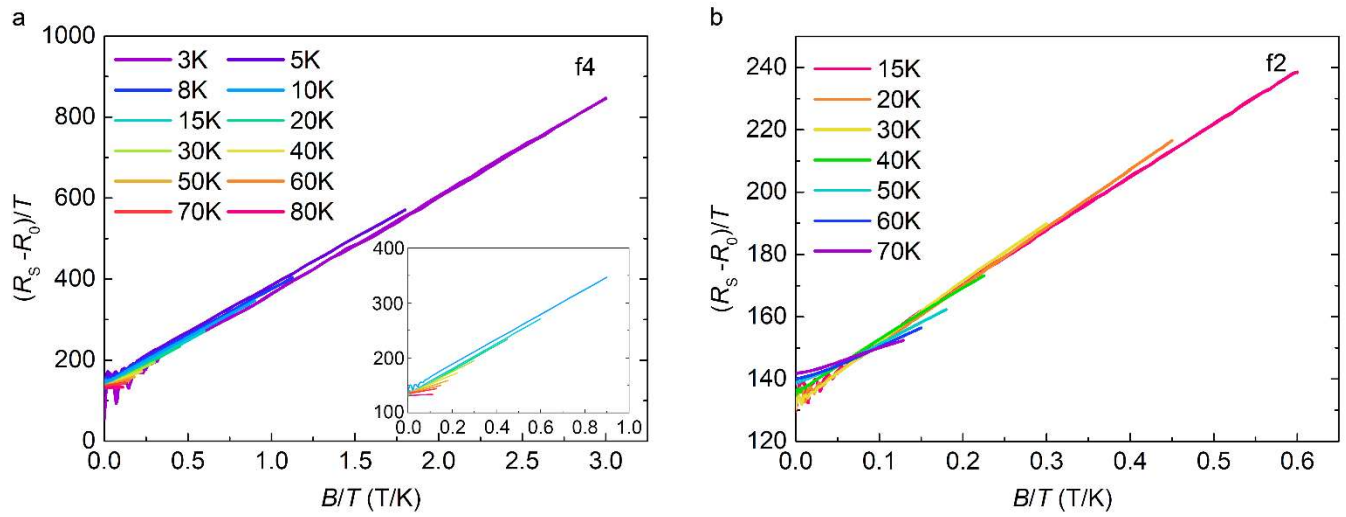


Fig. 3 | $B-T$ scaling in nanopatterned YBCO thin films. The resistance of f4 (a) and f2 (b) after subtracting the residual resistance $R_s(0,0)$, the remainder is divided by temperature, and plotted versus B/T . The insert is the detail of figure 3a from 10K to 80K. (The similar plots of other samples are shown in Supplementary Fig. 7).

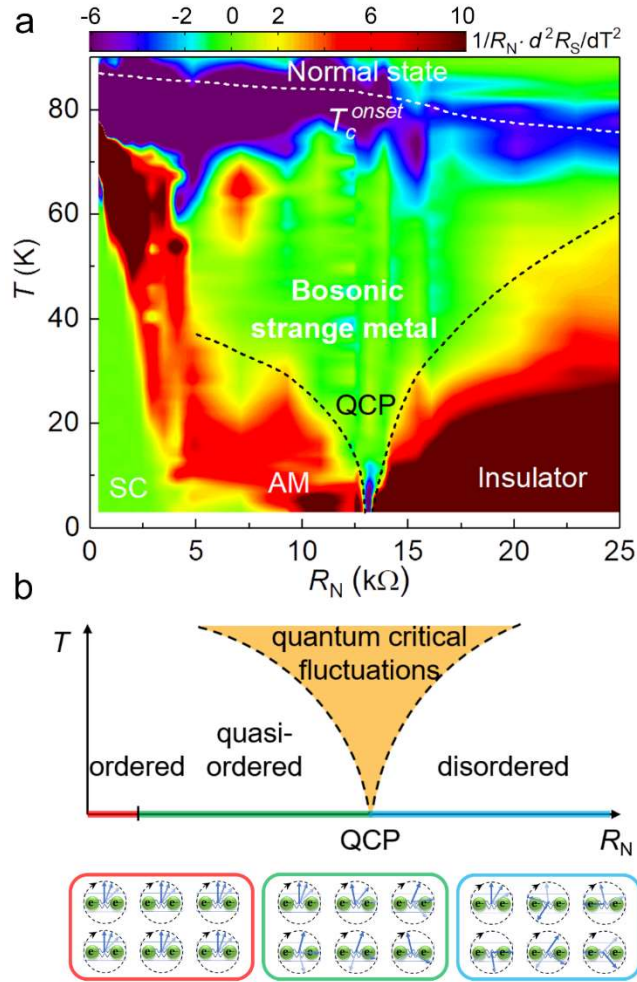
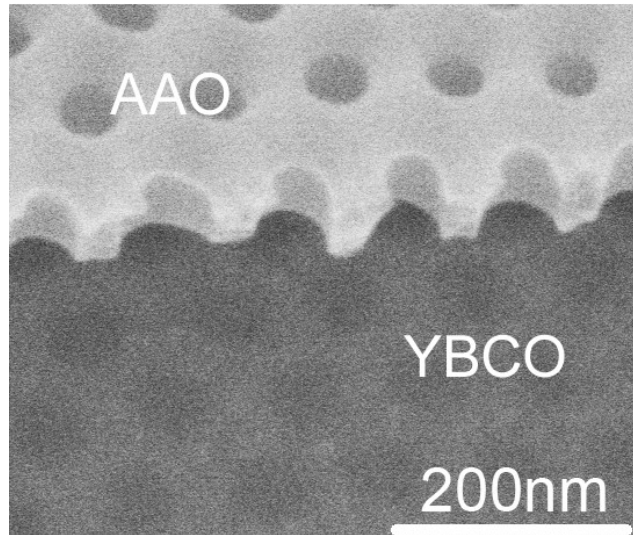
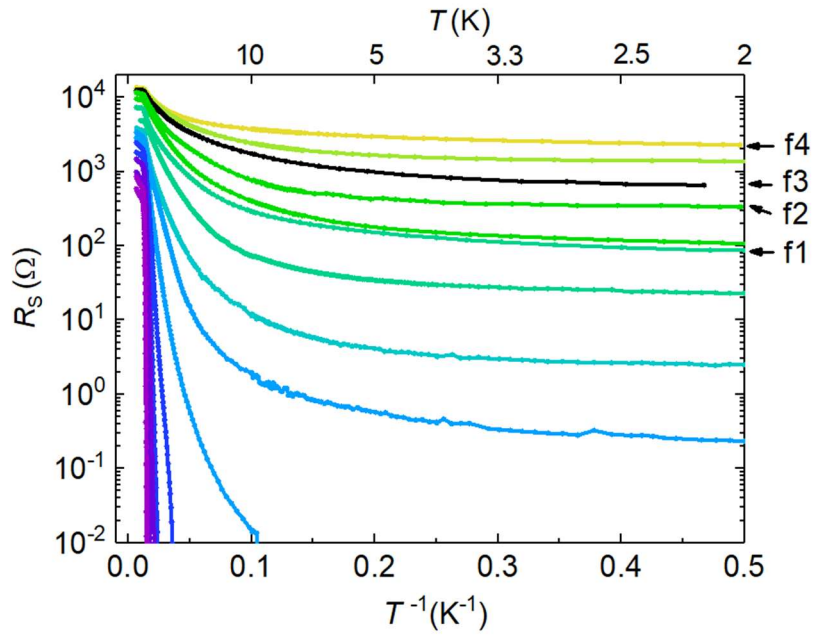


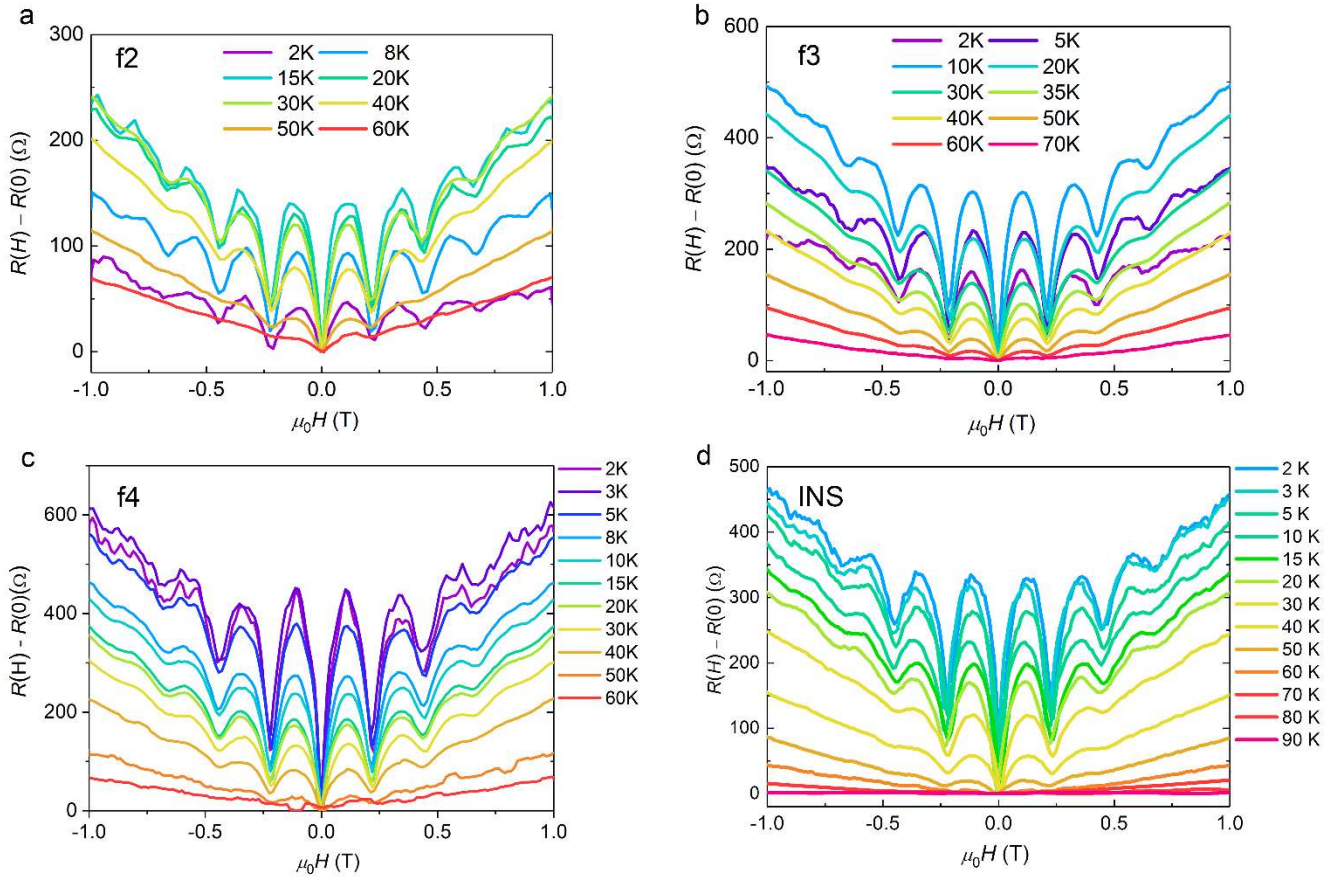
Fig. 4 | Phase diagram of nanopatterned YBCO thin films. (a) The normalized second derivative of resistance $1/R_N \cdot d^2 R_S / dT^2$ versus temperature and the normal state resistance R_N . The normal state and other states are separated by T_c^{onset} . The color scale conveys the second derivative of the sheet resistance as a function of temperature normalized to R_N . The central green region ($1/R_N \cdot d^2 R_S / dT^2$ close to zero), labelled bosonic strange metal, corresponds to the regime where the temperature dependence of the resistance is linear. Its boundaries (black dashed lines) are drawn where the deviations from linearity become significant. The bordering regions evolve into the bosonic insulator on the right and the anomalous metal phase (AM) in the low temperature limit. The superconducting phase (SC) is the green region to the right where $1/R_N \cdot d^2 R_S / dT^2$ approaches zero because R_S becomes very small. (b) Proposed idealized phase diagram illustrating a quantum critical region that corresponds to where strange metal behavior is observed. The bounding phases are the anomalous metal and bosonic insulator. The blue arrow stands for the SC order parameter. The ordered state (left), which is ordered both in space and time, corresponds to SC state. The quasi-ordered phase (middle), which is spatially ordered but disordered in time, corresponds to AM state. The disordered phase (right), which is disordered both in space and time, corresponds to insulator state. Near the critical point of quasi-ordered to disordered state, there is a quantum critical region where there is exotic T -linear resistance, corresponding to the bosonic strange metal.



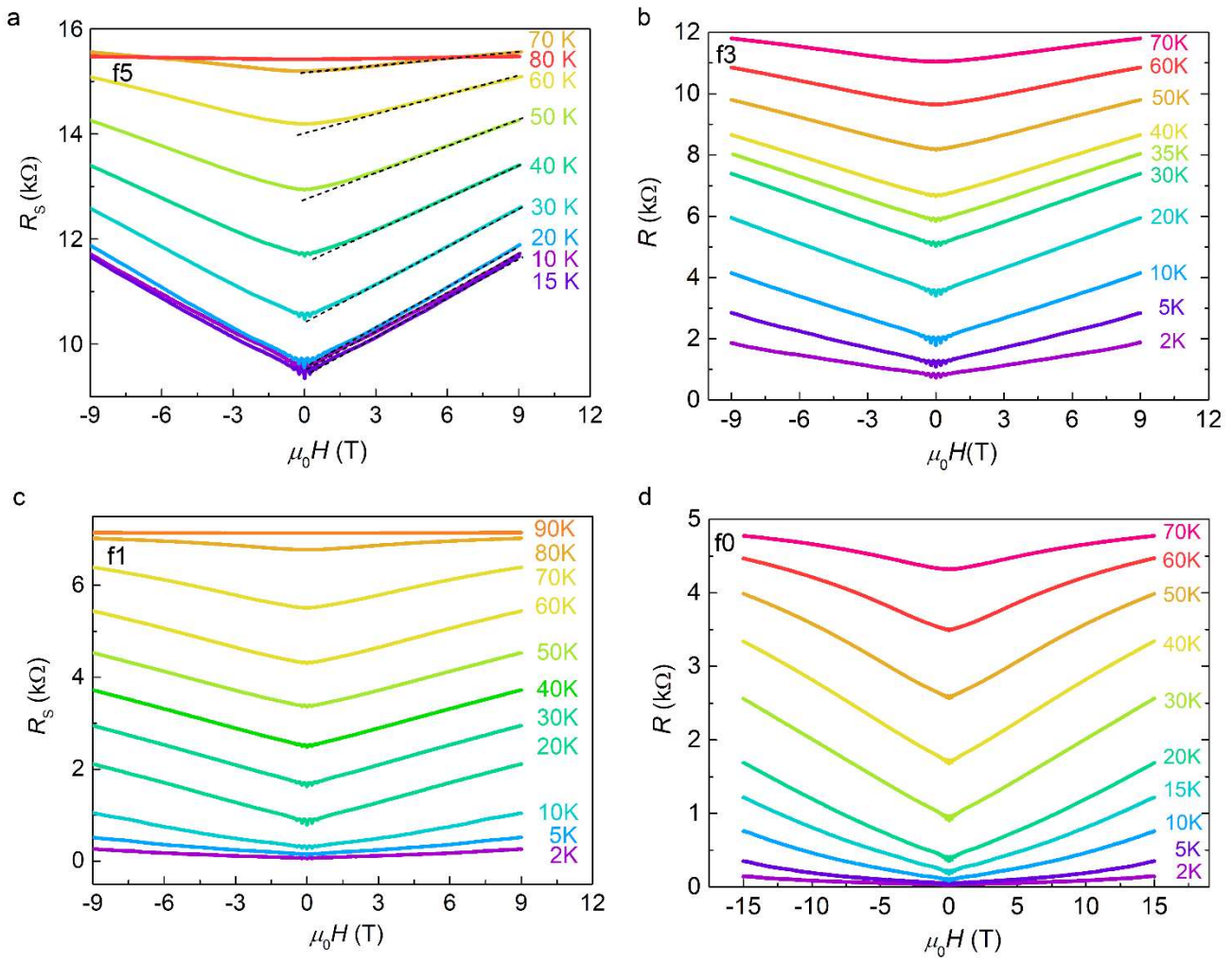
Supplementary Fig. 1 | The scanning electron microscopy of a nanopatterned YBa₂Cu₃O_{7-δ} (YBCO) thin film. The 12-nm-thick nanopatterned YBCO thin film was fabricated by reactive ion etching through an anodic aluminum oxide (AAO) membrane directly placed atop the YBCO. By RIE, the anodized aluminum oxide pattern of a triangular array of holes with ~70-nm diameter and ~103-nm period was duplicated onto the YBCO film.



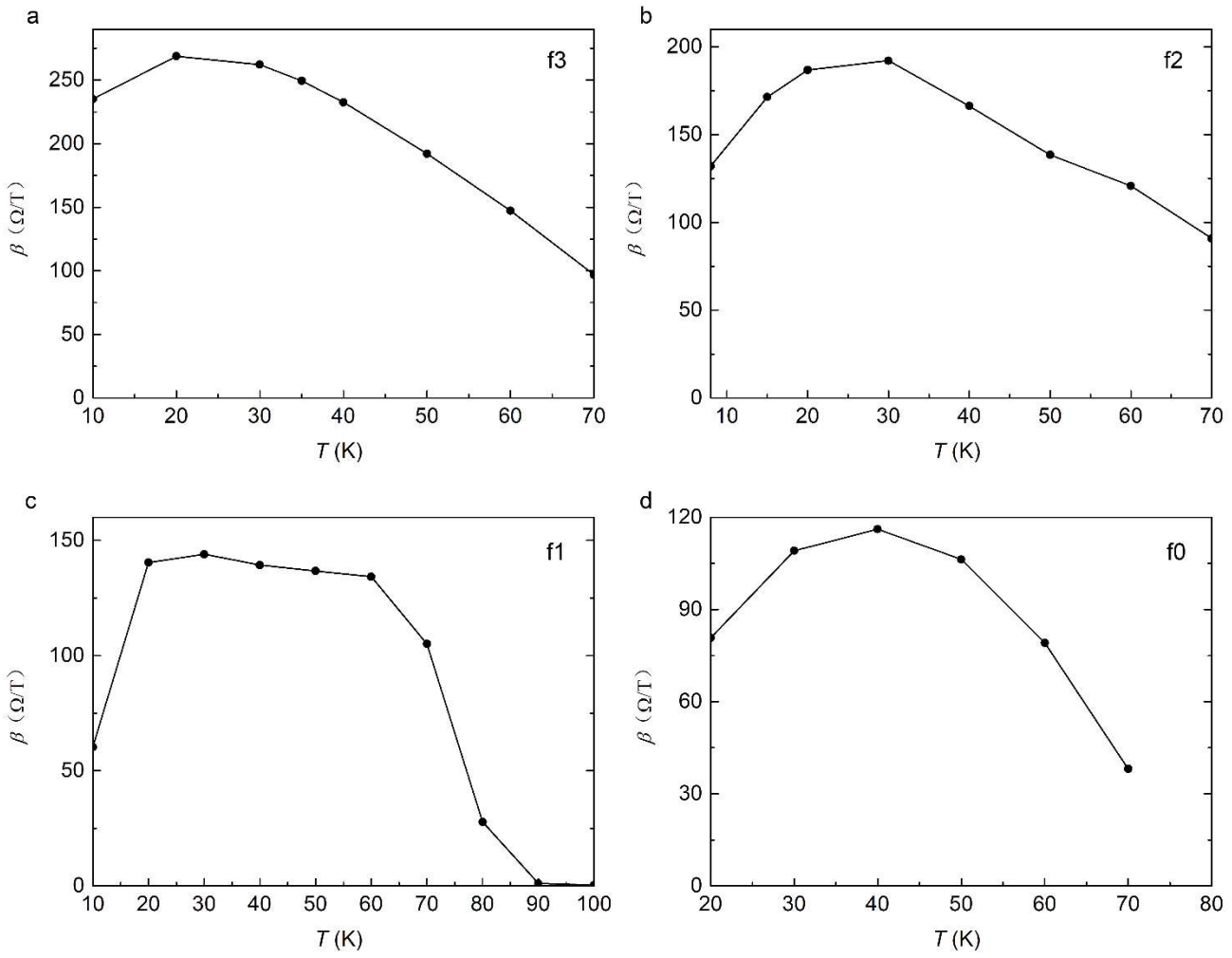
Supplementary Fig. 2 | Arrhenius plot of the $R_s(T)$ data of anomalous metallic state and superconducting state in Fig. 1a. The resistance of the four representative anomalous metallic state films f1, f2, f3 and f4 that have a linear temperature dependence over an extended range saturates at low temperatures on a $1/T$ scale. This saturation is a characteristic of the intermediate anomalous metallic state in the superconductor-insulator transition nanopatterned YBCO thin films.



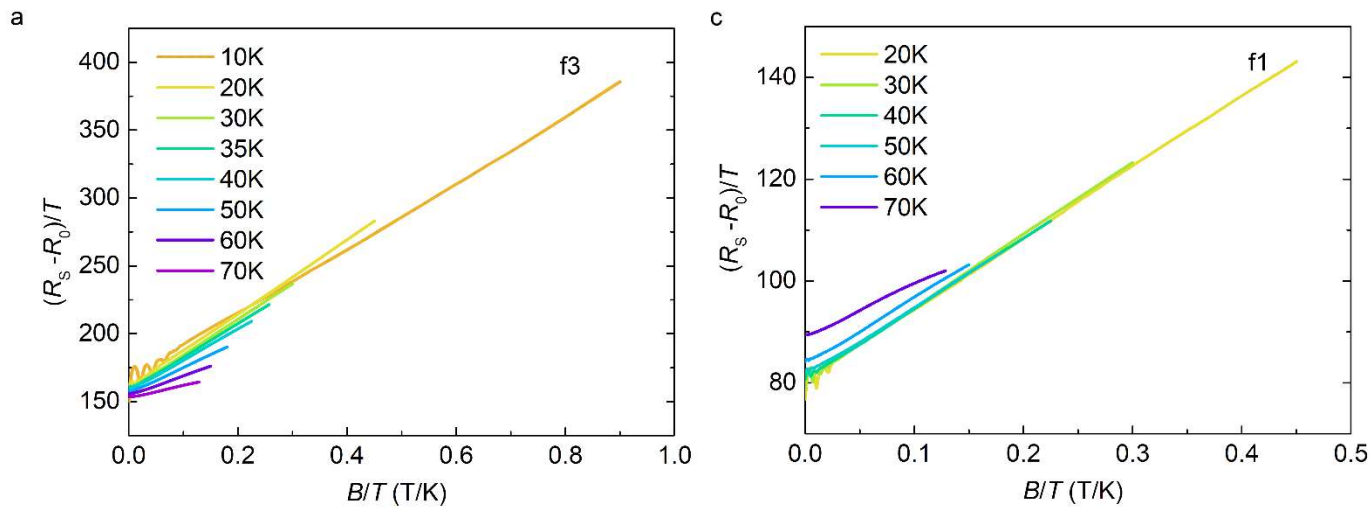
Supplementary Fig. 3 | The magneto-resistance oscillations in nanopatterned YBCO thin film. The full data of the magneto-resistance four representative YBCO thin films at various temperatures from 2K to 80K (a) f2 (b) f3 (c) f4 (d) a representative insulating state YBCO thin film. The observed oscillation period $\mu_0 H_0 \sim 0.225\text{T}$ is close to one superconducting flux per area of a unit cell that is $h/2eS$, where h is Planck's constant, e is the electron charge and S is $\sim 9200\text{ nm}^2$. These $h/2e$ magneto-resistance oscillations indicate that Cooper pairs participate in the transport below $T_c^{\text{onset}} \approx 84\text{K}$.



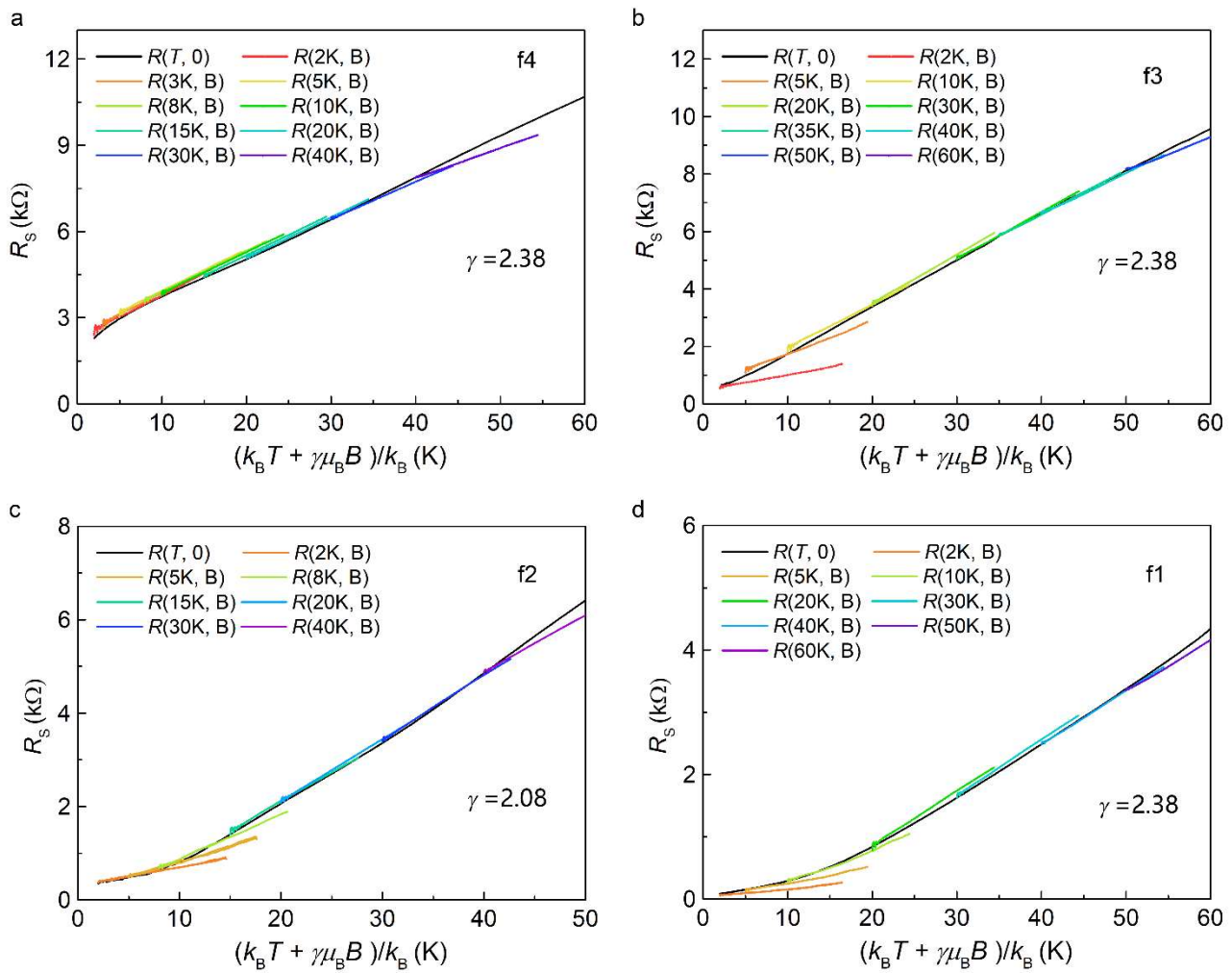
Supplementary Fig. 4 | scale-invariant B -linear resistance in nanopatterned YBCO thin films under perpendicular magnetic field. (a–d) The magnetoresistance for films: f5 (a), f3 (b), f1 (c), f0 (d).



Supplementary Fig. 5 | The slope of magnetoresistance β as a function of temperature: f3 (a), f2 (b), f1 (c) and f0 (d).



Supplementary Fig. 6 | B - T scaling in nanopatterned YBCO thin films of f3 (a) and f1 (b).



Supplementary Fig. 7 | The resistance and magneto-resistance of f4 (a), f3 (b), f2 (c) and f1 (d) as a function of $(k_B T + \gamma \mu_B B) / k_B$, where γ parameter can be estimated by adjusting it when the curves collapse best.

Extended Data Table 1 | Comparison between LSCO at p=0.21 and nanopatterned YBCO thin films near the anomalous metal to insulator transition.

	LSCO at p= 0.21	Nanopatterned YBCO thin films near the anomalous metal to insulator transition
<i>T</i> -linear resistivity $R_S = \alpha T + R_0$	ν	ν
Carriers	(Electrons) Fermions	(Cooper pairs) Bosons
α ($\Omega \cdot K^{-1}$)	15	157
A renormalized value η	$\eta = (2e^2/h) \cdot \alpha_F/T_F \approx 1,$ where $\hbar/\tau = \eta k_B T$	$\eta = (2e^2/h) \cdot \alpha_{cp}/T_c^{\text{onset}} \approx 1$